Analytica Chimica Acta 735 (2012) 96–106

Contents lists available at SciVerse ScienceDirect

Analytica Chimica Acta

journal homepage: www.elsevier.com/locate/aca

Synthesis and photophysical properties of water-soluble sulfonato-Salen-type Schiff bases and their applications of fluorescence sensors for Cu^{2+} in water and living cells

Li Zhou[a,1], Peiying Cai[b,1], Yan Feng[a], Jinghui Cheng[a], Haifeng Xiang[a,*], Jin Liu[b,*], Di Wu[a,*], Xiangge Zhou[a]

[a] Institute of Homogeneous Catalysis, College of Chemistry, Sichuan University, Chengdu 610041, China
[b] Laboratory of Stem Cell Biology, State Key Laboratory of Biotherapy, West China Hospital, Sichuan University, Chengdu 610064, China

GRAPHICAL ABSTRACT

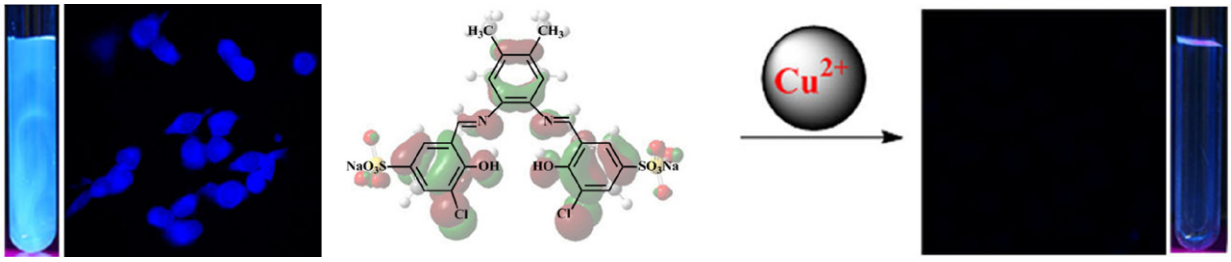

HIGHLIGHTS

- Sulfonate groups ensure good stability and solubility in water.
- Sulfonate groups have little effect on the photophysical properties.
- This is confirmed by the TD-DFT calculations and experimental results.
- The strong blue, green, or orange fluorescence is selectively quenched by Cu^{2+}.
- The ligands are sensitive fluorescence sensors for Cu^{2+} in water and living cells.

ARTICLE INFO

Article history:
Received 10 February 2012
Received in revised form 2 May 2012
Accepted 7 May 2012
Available online 23 May 2012

Keyword:
Salen
Schiff base
Cu^{2+} fluorescence sensor
Water soluble
Sulfonate group
TD-DFT calculation

ABSTRACT

A series of water-soluble sulfonato-Salen-type ligands derived from different diamines including 1,2-ethylenediamine (**Et-1**–**Et-4**), 1,2-cyclohexanediamine (**Cy-1** and **Cy-2**), 1,2-phenylenediamine (**Ph-1**–**Ph-3** and **PhMe-1**–**PhMe-4**), and dicyano-1,2-ethenediamine (**CN-1**) has been designed and prepared. Sulfonate groups of ligands ensure good stability and solubility in water without affecting their excited state properties. These ligands exhibit strong UV/Vis-absorption and blue, green, or orange fluorescence. Time-dependent-density functional theory calculations have been undertaken to reveal the influence of ligand nature, especially sulfonate groups, on the frontier molecular orbitals. Since their fluorescence is selectively quenched by Cu^{2+}, the sulfonato-Salen-type ligands can be used as highly selective and sensitive turn-off fluorescence sensors for the detection of Cu^{2+} in water and fluorescence imaging in living cells.

* Corresponding authors. Tel.: +86 28 8541 229; fax: +86 28 8541 2291.
E-mail address: xianghaifeng@scu.edu.cn (H. Xiang).
[1] These authors contributed equally to the work.

0003-2670/$ – see front matter © 2012 Elsevier B.V. All rights reserved.
http://dx.doi.org/10.1016/j.aca.2012.05.022

1. Introduction

During the past two decades, considerable attention has been paid to the chemistry of the Schiff bases and their metal complexes containing nitrogen, oxygen and sulfur donor atoms [1–6]. Especially, Salen, a particular class of tetradentate [OˆNˆNˆO] chelating bis-Schiff base (Scheme 1), can be synthesized by the condensation of salicylaldehyde or its derivatives with 1,2-diamines [7–10]. Due to their stabilities, biological activities, and photophysical properties, Salen-type ligands and their metal complexes have exhibited many potential applications in many fields, such as catalysts [2,4,7,8,10], DNA cleavage [11,12], optical materials [1,3,6], magnetic materials [6,9], and sensors [5]. For example, Zn(II) [13], B(III) [14], Al(III) [15], and Pt(II) Salen [16–19] complexes with excellent luminescent properties and good thermal stabilities have been used as emitters in the application of organic light-emitting diodes (OLEDs). In addition, since Salen-type ligands with big π-conjugated system usually exhibit strong fluorescence with or without various metal ions [1–10], there are many reports on the Salen-type or analogous amine fluorescence sensors [5] for ions, such as Zn^{2+} [20–22], Mg^{2+} [23], Cu^{2+} [20,24–26], Al^{3+} [24], La^{3+} [27], V [28], and I^{-1} [29].

Our previous work demonstrated that introducing sulfonate groups to Salen-type ligands could improve their solubility in water and their complexes were used as aqueous homogeneous catalysts in some coupling reactions [30,31]. Nevertheless, there are still rare studies on the photophysical properties of water-soluble sulfonato-Salen-type ligands (SSLs) in the literature and the studies on optical sulfonato materials are mostly focused on tetrakis(*p*-sulfonatophenyl)porphyrin [32,33]. In the present work, we describe the synthesis and photophysical properties of a series of luminescent SSLs with different bridge of 1,2-ethylenediamine (**Et-1**–**Et-4**), 1,2-cyclohexanediamine (**Cy-1** and **Cy-2**), 1,2-phenylenediamine (**Ph-1**–**Ph-3** and **PhMe-1**–**PhMe-4**), and dicyano-1,2-ethenediamine (**CN-1**) (Scheme 1). The presence of sulfonate groups in SSLs ensures not only good stability but also solubility in water without affecting their excited state properties. These SSLs exhibit strong UV/Vis-absorption at 200–400 nm and blue, green, or orange fluorescence with quantum yield (Φ) up to 0.56 in water. The influence of the ligand nature on the UV-absorption and fluorescence is evaluated by introducing different chemical groups to the ligand, which is explained by the time-dependent-density functional theory (TD-DFT) calculations. The fluorescence response of SSLs toward various metal ions is fully investigated. Various metal ions lead to a slight fluorescence quenching or enhancement, but only Cu^{2+} leads to an efficient fluorescence quenching. Therefore, the SSLs can be used as highly selective and sensitive turn-off fluorescence sensors for Cu^{2+} in water and fluorescence imaging in living cells.

2. Experimental

2.1. Materials and instrumentation

All reagents were purchased from commercial suppliers and used without further purification. All the ligands were prepared according to previous reports (See the Supporting information) [34,35]. ^{1}H NMR (400 MHz) spectra were recorded in [D6]DMSO. Chemical shifts are reported in ppm using tetramethylsilane as internal standard. UV/Vis absorption spectra were recorded using a UV 765 spectrophotometer with quartz cuvettes of 1 cm pathlength. Fluorescence spectra were obtained using FluoroMax-4 Spectrofluorophotometer (HORIBA Jobin Yvon) linked to a Pentium PC running SpectraCalc software package at 298 K. The slit width was 5.0 nm for both excitation and emission. The photon multiplier voltage was 400 V. Samples in solution and powder were contained in 10.0 mm path length quartz cuvettes (3.5 mL volume) and quartz tube, respectively.

2.2. Measurement of fluorescence quantum yield (Φ)

Φ was measured by the optical dilute method of Demas and Crosby [36] with a standard of quinine sulfate ($\Phi_r = 0.55$, quinine in 0.05 mol dm^{-3} sulfate) calculated by: $\Phi_s = \Phi_r(B_r/B_s)(n_s/n_r)^2(D_s/D_r)$, where the subscripts s and r refer to the sample and reference standard solution respectively; n is the refractive index of the solvents; D is the integrated intensity. The excitation intensity B is calculated by: $B = 1–10^{-AL}$, where A is the absorbance at the excitation wavelength and L is the optical path length ($L = 1$ cm in all cases). The refractive indices of the solvents at room temperature are taken from standard source. Errors for Φ values (±10%) are estimated.

2.3. Measurement of metal ion sensing

Each metal ion titration experiment was started with ligand (3 mL) of known concentration (1.0×10^{-6} mol dm^{-3} in water). $Cu(NO_3)_2$ salt and other various metal salts (nitrate, 1.0×10^{-4} mol dm^{-3} in H_2O) were used for the titration. All types of florescent measurement (excited at 370 nm) were monitored 10 min after addition of the metal salt to the ligand solutions.

2.4. Computational details

Calculations were carried out using the Gaussian 03 software package (B3LYP 6-31G(d,p)) [37]. For the atoms of organic ligands, the standard split-valence basis sets 6-31G(d,p) augmented with polarization d-functions for the non-hydrogen atoms and p-functions for the hydrogen atoms were used. Full geometry optimization of all the ligands corresponding to the minima on the potential energy surface (PES) was conducted until a gradient of 10^{-5} at.u. The spin multiplicities of the ligands were set equal to 1. The charges of the ligands with and without sulfonate groups were set equal to −2 and 0, respectively. The other parameters were set to default values.

2.5. Cell culture methods and confocal imaging

The imaging of A549 cells was finished by Fluorescence Vertical Microscope AX10. A549 cells were cultured in DMEM supplemented with 10% fetal bovine serum, penicillin(100 units mL^{-1}), streptomycin(100 mg mL^{-1}) and 5% CO_2 at 37 °C. After removing the incubating media and rinse with 1 × PBS for three times, the cells were incubated with **PhMe-4** (20 μmol dm^{-3}) or **PhMe-4** + Cu^{2+} (20 μmol dm^{-3}) in PBS for 20 min at room temperature. Then, the cells was washed three times with PBS and imaged with confocal microscope (excited at 370 nm).

3. Results and discussion

3.1. Synthesis and features of the ligands

For comparison, three Salen-type ligands without sulfonate groups, *N*,*N*′-*bis*(salicylidene)-1,2-ethylenediamine (**Salen**), *N*,*N*′-*bis*(salicylidene)-1,2-cyclohexanediamine (**CySalen**), and *N*,*N*′-*bis*(salicylidene)-1,2-phenylenediamine (**Salphen**) (Scheme 1), were prepared according to previous reports [34,35]. The reactions of 2 equiv. of appropriate 1,2-diamine with 1 equiv. of substituted salicylaldehydes in ethanol gave the corresponding ligands, which were recrystallized from ethanol resulting in **Salen**, **CySalen**, and **Salphen** as yellow, yellow, and orange crystal, respectively. They

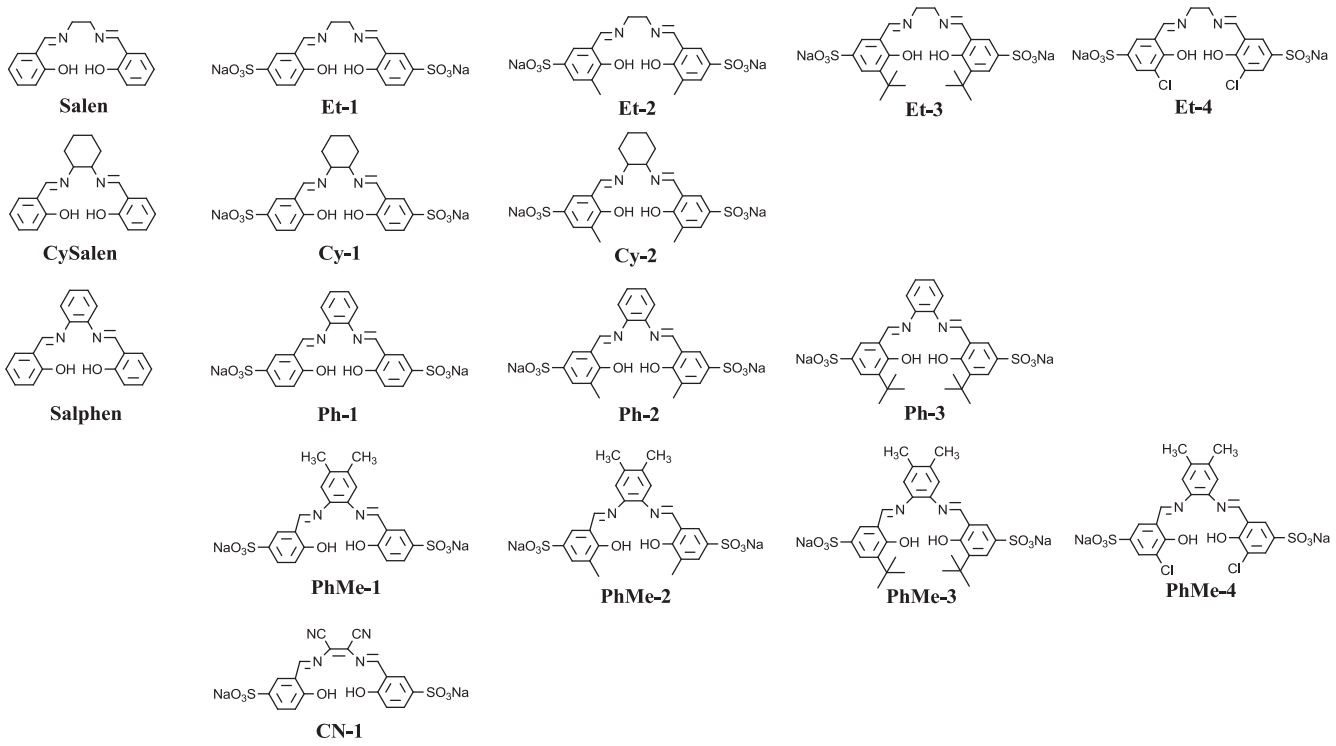

Scheme 1. Chemical structures of Salen-type ligands used in this work.

have good solubility in organic solvent, such as ethanol, CH_3CN, and DMF, and bad solubility in water.

Except *N*,*N*′-*bis*(5-sulfonatosalicylidene)-dicyano-1,2-ethenediamine disodium salt (**CN-1**) [13], all other SSLs were prepared in moderate to high yields ranging from 57 to 85% by the condensation of 1 equiv. of different diamines with corresponding 2 equiv. 5-sulfonatosalicylaldehydes in the same procedure. For example, *N*,*N*′-*bis*(5-sulfonatosalicylidene)-1,2-phenylenediamine disodium salt (**Ph-1**) was synthesized from the starting material of salicylaldehyde in a four-step reaction [34,35], as shown in Scheme 2.

The sulfonate groups of SSLs ensure not only good stability but also solubility in water [30–35,38]. All the solid-state SSLs and their aqueous solutions are stable in air within several months. In order to identify the chemical structure of the SSLs, various attempts to grow single crystal were carried out but failed. Recently, the single crystal of *N*,*N*′-*bis*(5-sulfonatosalicylidene)-1,2-diaminoethanenickel(II) disodium salt complex was succeed to grow, whose single-crystal X-ray diffraction structure shows that the ligand has remained intact and coordinates the Ni^{2+} cation in square-planar geometry, as expected for tetradentate Salen-type complexes, and the dimmers of complexes are organized in chains held together by a complex arrangement of Na^+ cations [35].

3.2. UV/Vis absorption spectroscopy

The UV/Vis absorption spectral data of all the ligands are listed in Table 1. Without sulfonate groups, **Salen**, **CySalen**, and **Salphen** in DMF have relatively intense absorption bands centered at $\lambda_{abs,max}$ = 315–331 nm (molar extinction coefficient, $\varepsilon = 1.4–2.5 \times 10^4\ dm^3\ mol^{-1}\ cm^{-1}$), which are assigned to $\pi \rightarrow \pi^*$ transition involving molecular orbitals essentially localized on the C=N group and the benzene ring (Table 1 and Fig. S1 in the Supporting Information) [20,24,39–41]. The

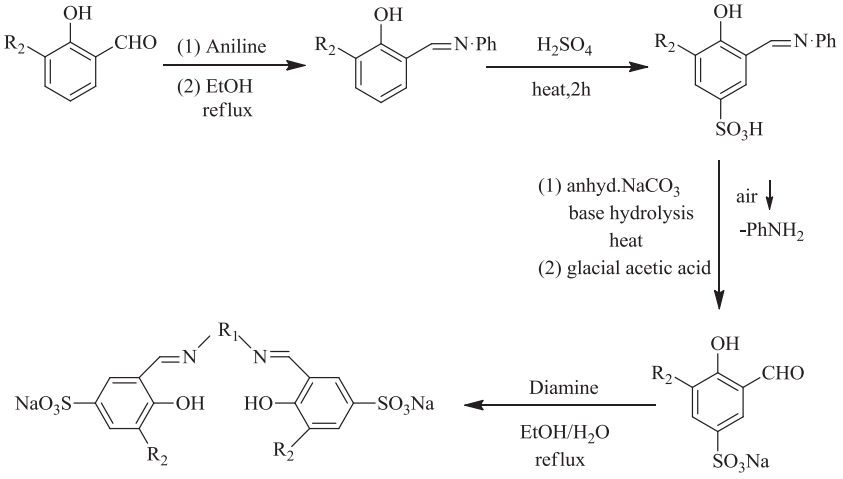

Scheme 2. Synthetic route of the SSLs.

Table 1
Photophysical data of the ligands at room temperature.

Ligand	Medium	λ_{abs} [nm] (ε [dm^3 mol^{-1} cm^{-1}])	λ_{em} [nm]	Φ
Salen	DMF	266 (2.49×10^4); 315 (2.43×10^4); 402 (1.59×10^3)	420	0.057
	CH_3CN	274 (2.16×10^4); 352 (2.45×10^3); 396 (1.16×10^3)	450	
CySalen	DMF	253 (1.10×10^4); 318 (6.9×10^3); 400 (2.70×10^2)	428	0.097
	CH_3CN	275 (2.10×10^4); 356 (2.86×10^3); 400 (2.01×10^3)	440	
Salphen	DMF	272 (2.76×10^4); 331 (2.36×10^4)	496	0.19
	CH_3CN	274 (1.97×10^4); 335 (1.06×10^4)	457	
Et-1	H_2O	196 (1.39×10^5); 234 (3.22×10^4); 254 (1.43×10^4); 306 (2.18×10^3); 371 (4.11×10^3)	491	0.055
	DMF	265 (8.09×10^3); 323 (6.03×10^3); 402 (9.70×10^2)	442	0.068
	CH_3CN	235 (1.54×10^4); 305 (6.56×10^3)	400	0.069
	Powder		494	
Et-2	H_2O	239 (2.87×10^4); 258 (1.93×10^4); 332 (5.95×10^3); 387 (5.27×10^3)	507	0.050
	DMF	268 (1.13×10^4); 328 (4.02×10^3); 402 (6.51×10^2)	455	0.044
	CH_3CN	240 (8.89×10^3); 282 (1.34×10^4)	408	0.095
Et-3	H_2O	194 (1.92×10^5); 259 (1.09×10^4); 334 (3.55×10^3)	512	0.081
	DMF	268 (9.70×10^3); 328 (4.13×10^3); 416 (3.41×10^2)	458	0.046
	CH_3CN	261 (1.27×10^4); 335 (5.97×10^3)	412	0.068
Et-4	H_2O	194 (1.77×10^5); 239 (4.48×10^4); 259 (1.47×10^4); 379 (1.03×10^4)	503	0.044
	DMF	266 (7.02×10^3); 326 (1.90×10^3); 407 (4.92×10^3)	483	0.12
	CH_3CN	260 (9.74×10^3); 288 (3.54×10^3); 337 (2.73×10^3)	406	0.15
Cy-1	H_2O	196 (2.05×10^5); 256 (1.45×10^4); 327 (3.02×10^3); 375 (3.55×10^3)	493	0.050
	DMF	265 (1.94×10^4); 321 (1.70×10^4); 416 (7.61×10^2)	441	0.052
	CH_3CN	235 (1.52×10^4); 308 (5.41×10^3)	405	0.11
	Powder		521	
Cy-2	H_2O	193 (1.33×10^5); 241 (1.57×10^4); 259 (1.29×10^4); 332 (4.54×10^3); 386 (3.16×10^3)	515	0.010
	DMF	268 (1.73×10^4); 328 (7.39×10^3); 415 (4.35×10^2)	472	0.061
	CH_3CN	263 (1.27×10^4); 310 (5.07×10^3)	408	0.062
Ph-1	H_2O	196 (2.17×10^5); 292 (1.05×10^4); 314 (8.77×10^3); 329 (8.06×10^3); 369 (4.84×10^3)	431	0.33
	DMF	294 (1.30×10^4); 316 (1.18×10^4); 375 (1.51×10^3)	437	0.56
	CH_3CN	296 (1.68×10^4); 327 (1.51×10^3)	457	0.25
	Powder		551	
Ph-2	H_2O	196 (2.07×10^5); 259 (1.35×10^4); 294 (1.02×10^4); 329 (8.99×10^3); 372 (4.13×10^3)	443	0.24
	DMF	285 (1.64×10^4); 297 (1.71×10^4); 321 (1.55×10^4); 335 (1.53×10^4); 382 (4.05×10^3)	473	0.18
	CH_3CN	292 (1.32×10^4); 319 (8.04×10^3); 333 (7.24×10^3)	467	0.29
Ph-3	H_2O	193 (1.43×10^5); 259 (1.54×10^4); 294 (4.52×10^3); 332 (6.25×10^3)	446	0.029
	DMF	285 (2.74×10^4); 332 (2.52×10^4); 348 (2.39×10^4)	470	0.031
	CH_3CN	302 (1.54×10^4); 336 (2.31×10^3)	466	0.071
PhMe-1	H_2O	196 (2.11×10^5); 301 (8.42×10^3); 322 (8.42×10^3); 337 (7.71×10^3); 371 (4.31×10^3)	429	0.56
	DMF	295 (1.72×10^4); 324 (2.08×10^4); 338 (1.98×10^4); 376 (9.77×10^3)	457	0.32
	CH_3CN	282 (1.27×10^4); 333 (1.37×10^3)	454	0.35
PhMe-2	H_2O	258 (1.96×10^4); 306 (8.06×10^3); 335 (9.26×10^3); 374 (5.44×10^3)	439	0.11
	DMF	270 (1.01×10^4); 339 (8.08×10^3); 380 (5.35×10^3)	472	0.11
	CH_3CN	259 (1.07×10^4); 333 (4.73×10^3)	462	0.22
PhMe-3	H_2O	259 (5.61×10^3); 326 (3.85×10^3); 339 (3.51×10^3); 367 (1.74×10^3)	445	0.19
	DMF	278 (7.04×10^3); 301 (7.52×10^3); 325 (8.51×10^3); 341 (8.78×10^3); 383 (3.84×10^3)	472	0.27
	CH_3CN	263 (6.22×10^3); 284 (4.39×10^3); 323 (3.54×10^3); 338 (3.54×10^3)	464	0.56
PhMe-4	H_2O	198 (2.43×10^5); 238 (2.16×10^4); 318 (1.20×10^4); 377 (7.81×10^3)	436	0.45
	DMF	270 (7.83×10^3); 299 (1.10×10^4); 325 (1.62×10^4); 341 (1.58×10^4); 407 (1.89×10^3)	464	0.48
	CH_3CN	286 (1.74×10^4); 332 (1.39×10^4)	454	0.60
CN-1	H_2O	252 (1.33×10^4); 334 (1.64×10^4); 374 (1.52×10^4); 392 (1.33×10^4)	507	0.30
	DMF	334 (7.85×10^3); 381 (1.31×10^4); 402 (1.06×10^4)	569	0.092
	CH_3CN	337 (4.9×10^3); 371 (6.55×10^3); 394 (5.05×10^3)	563	0.035

lower intensity absorption bands ($\varepsilon = 1.67 \times 10^3$, 5.80×10^2, and 3.39×10^3 dm^3 mol^{-1} cm^{-1} for **Salen**, **CySalen**, and **Salphen**, respectively) in the $\lambda_{abs,max}$ = 380–420 nm region respond for pale yellow, pale yellow, and yellow color of **Salen**, **CySalen**, and **Salphen**, respectively, assigned to $n \rightarrow \pi^*$ transition involving molecular orbitals of the C=N chromophore and the benzene ring [20,24,39–41]. **CySalen** with the bridge of 1,2-cyclohexanediamine has similar absorption spectrum with **Salen**, but **Salphen** with the bridge of 1,2-phenylenediamine exhibits a larger π charge delocalization over the salicylidene and phenylene aromatic rings than **Salen** and **CySalen**, resulting in a more intense, broader and bathochromic-shifted (red-shifted) band in the absorption spectrum.

As examples, the absorption spectra of *N*,*N*′-*bis*(5-sulfonatosalicylidene)-1,2-ethylenediamine disodium salt (**Et-1**), *N*,*N*′-*bis*(5-sulfonatosalicylidene)-1,2-cyclohexanediamine disodium salt (**Cy-1**), **Ph-1**, and *N*,*N*′-*bis*(5-sulfonatosalicylidene)-4,5-dimethyl-1,2-phenylenediamine disodium salt (**PhMe-1**) with the different diaminobridges in water are given in Fig. 1. Their

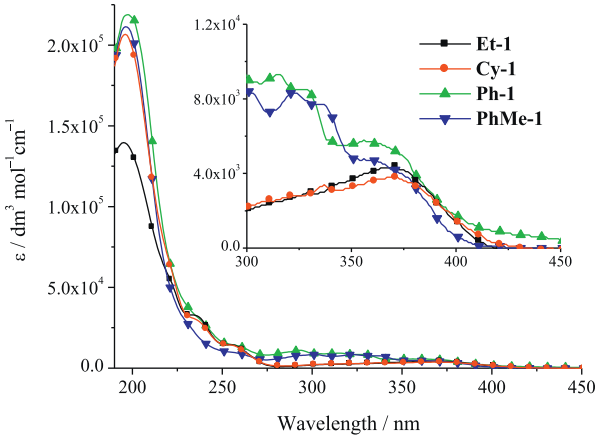

Fig. 1. Absorption spectra of **Et-1**, **Cy-1**, **Ph-1**, and **PhMe-1** (1.0×10^{-5} dm^3 mol^{-1}) in water.

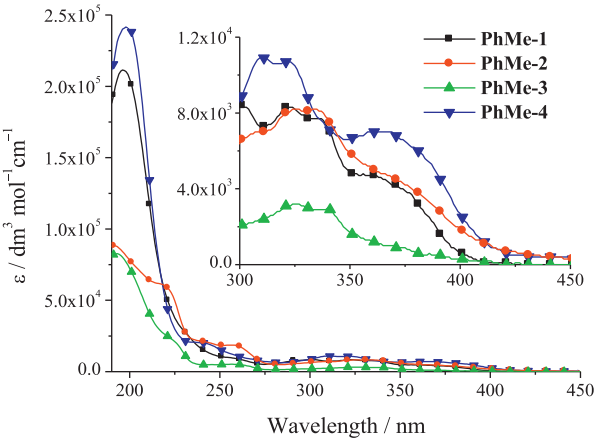

Fig. 2. Absorption spectra of **PhMe-1**, **PhMe-2**, **PhMe-3**, and **PhMe-4** (1.0×10^{-5} dm^3 mol^{-1}) in water.

absorption peaks (or shoulder) appear at ~196, 235, 258, 320, and 370 nm, resulting in that the solutions are colorless. The isolated benzene ring exhibits three characteristic absorptions at $\lambda_{abs,max}$ = 184, 204 and 256 nm, assigned to $\pi \rightarrow \pi^*$ transitions [40]. Substitutions on the benzene ring by auxochromes and chromophores shift these bands to the red. Therefore, the absorption bands at high energy (λ < 275 nm) are assigned to $\pi \rightarrow \pi^*$ transition in phenolic ring. The absorption bands with low energy at $\lambda_{abs,max}$ = 320 and 370 nm are attributed to the $\pi \rightarrow \pi^*$ and $n \rightarrow \pi^*$ transition in the C=N group and the benzene ring, respectively, like the ligands without sulfonate groups [20,24,39–41]. The similar substitution effects of the diamine bridge are observed. **Et-1** and **Cy-1** with the bridge of 1,2-ethylenediamine and 1,2-cyclohexanediamine, respectively, have almost same absorption spectra, but **Ph-1** and **PhMe-1** with 1,2-phenylenediamine bridge exhibit more intense, broader and red-shifted absorption bands (Fig. 1). Compared with **Ph-1**, the introduction of methyl groups to 1,2-phenylenediamine bridge **(PhMe-1)** has little effect on absorption spectrum. In order to investigate the substitution effect in phenolic ring, the absorption spectra of **PhMe-1**–**PhMe-4** are examined (Fig. 2). *N*,*N*′-*bis*(3-Methyl-5-sulfonatosalicylidene)-4,5-dimethyl-1,2-phenylenediamine disodium salt (**PhMe-2**) with methyl groups in phenolic ring has similar absorption with **PhMe-1**, but *N*,*N*′-*bis*(3-tertbutyl-5-sulfonatosalicylidene)-4,5-dimethyl-1,2-phenylenediamine disodium salt (**PhMe-3**) with steric hindrance of *t*-butyl groups exhibits less intense absorption than **PhMe-1**. *N*,*N*′-*bis*(3-Chlorine-5-sulfonatosalicylidene)-4,5-dimethyl-1,2-phenylenediamine disodium salt (**PhMe-4**) with electron-donate substituents of Cl atom shows more intense absorption than **PhMe-1**. Compared with those of the ligands without sulfonate groups, the absorption spectra of the **Et-1**, **Cy-1**, and **Ph-1** show small changes, indicting that the sulfonate groups have little effect on the properties of absorption (the more detailed information is discussed in the later part), consistent with the former reported optical sulfonato materials [32,33,38].

3.3. Fluorescence spectroscopy

The fluorescent emission data of the ligands are listed in Table 1. At room temperature, all the Schiff bases in the present work emit blue, green, or orange light upon the UV excitation. Generally, salicylaldimines can exist as a tautomerization of keto-amine and phenol-imine form through intramolecular proton transfer [3,42–44]. Similarly, **Salphen** also has an intra molecular hydrogen transfer (Scheme S1) between the phenolic O—H and the nitrogen of the imine and yields a red shift from blue

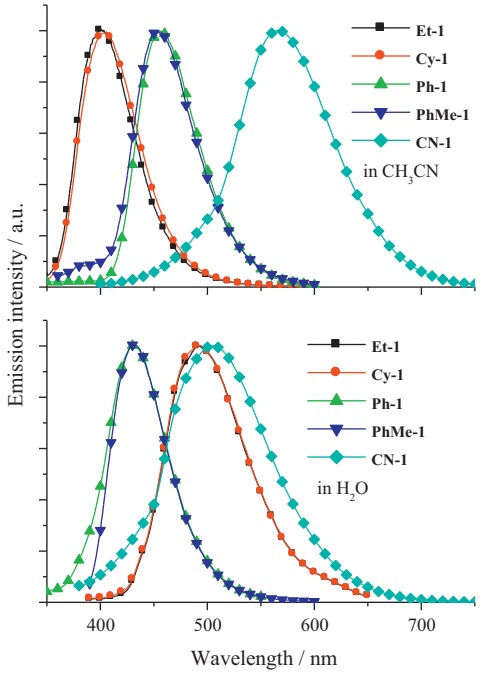

Fig. 3. Normalized fluorescence spectra of **Et-1**, **Cy-1**, **Ph-1**, **PhMe-1**, and **CN-1** in CH_3CN and water.

emission ($\lambda_{em,max}$ = 457 nm) of phenol-imine form in CH_3CN to blue-green emission ($\lambda_{em,max}$ = 496 nm) of keto-amine form in DMF (Table 1 and Fig. S2), which is consistent with the former reported experiment result [3,21] and theoretical calculation [41,44]. Strangely, the emission band of **Salen** in DMF is centered at $\lambda_{em,max}$ = 420 nm and gives a hypochromatic (blue) shift compared with that ($\lambda_{em,max}$ = 450 nm) of **Salen** in CH_3CN.

The absorption, excitation, and emission spectra of **Ph-1** in water are shown in Fig. S3. The excitation spectrum of **Ph-1** has complicated vibronic bands centered at $\lambda_{em,max}$ = 293, 329, and 369 nm, almost as same as its absorption spectrum. However, without symmetry with its excitation spectrum or absorption spectrum, the emission spectrum of **Ph-1** lacks vibronic bands with only one peak at $\lambda_{em,max}$ = 431 nm, even though excitated at different wavelength of 293, 329, and 369 nm, suggesting that the vibronic structure of ground state is different from that of the excited states. This might be explained by the single-crystal X-ray diffraction structure of Salen-type ligands [43,45–48]. For example, the two phenolic rings in **Salphen** are not in one plane. The dihedral between the plane of one phenolic ring and the plane consisting the central phenylenediamine and the other phenyl ring is about 28° (Figs. S4 and S5), indicating that the molecular structure of **Salphen** is not rigidly but rotary. This molecular rotation of **Salphen** might lose the energy of excited states to lead to the lack of vibronic structure in emission spectrum, which could be frozen at low temperature to reappear the renascence of vibronic structure in emission spectrum [41]. The emission spectrum of **Ph-1** ($\lambda_{em,max}$ = 457 nm) in CH_3CN is similar with that of **Salphen** ($\lambda_{em,max}$ = 457 nm), revealing that the sulfonate groups have little effect on the fluorescence property.

In order to classify the relationship between the emission properties and chemical structures, the emission spectra of **Et-1**, **Cy-1**, **Ph-1**, **PhMe-1**, and **CN-1** with the different diaminobridges in CH_3CN and water (1.0×10^{-6} mol dm^{-3}) are depicted in Fig. 3. At room temperature, **Et-1**, **Cy-1**, **Ph-1**, and **PhMe-1** in CH_3CN exhibit broad fluorescence band centered at λ_{max} = 400, 405, 457, and 454 nm, respectively, mostly attributed to $\pi \rightarrow \pi^*$ transition [39–41]. It is well known that the π-conjugation enhancement

should lead to a considerable decrease in the energy gap between the highest occupied molecular orbital (HOMO) and lowest unoccupied molecular orbital (LUMO), resulting in a red shift in emission spectrum, which is confirmed by that the emission peak of **Salphen** is at $\lambda_{em,max}$ = 496 nm and that of **Salen**, **CySalen** is at λ_{max} = 420 and 428 nm, respectively (Fig. S6). The further analysis of the experimental data of **Et-1**, **Cy-1**, **Ph-1**, and **PhMe-1** reveals the same effect (Table 1 and Fig. 3). **Et-1** and **Cy-1** with the bridge of 1,2-ethylenediamine and 1,2-cyclohexanediamine, respectively, have almost same emission spectra centered at 400 and 405 nm (in CH_3CN), respectively. Like **Salphen**, **Ph-1** and **PhMe-1** with 1,2-phenylenediamine bridge show red shifts in emission spectra with the peak at $\lambda_{em,max}$ = 457 and 454 nm, respectively. Interestedly, the emission spectra of **Ph-1** and **PhMe-1** in H_2O exhibit blue shifts from in CH_3CN, but the emission spectra of **Et-1** and **Cy-1** in H_2O exhibit red shifts from in CH_3CN (Fig. 3). Fig. S7 shows the substitution effect in phenolic ring on the emission spectra. **PhMe-2**, **PhMe-3**, and **PhMe-4** with methyl, *t*-butyl, and Cl groups, respectively, in phenolic ring and **PhMe-1** have similar emission spectra centered at $\lambda_{em,max}$ = 429–445 nm, indicating that those substitutions in phenolic ring have little effect on the energy gap of SSLs (the more detailed information is discussed in the later part). Replacing 1,2-phenylenediamine bridge by dicyano-1,2-ethenediamine bridge, the fluorescence of **CN-1** gives a further red shift to $\lambda_{em,max}$ = 563 nm in CH_3CN (Fig. 3).

All fluorescence quantum yields of the ligands in solution are measured by the optical dilute method of Demas and Crosby [36] with a standard of quinine sulfate (Φ_r = 0.55, quinine in 0.05 mol dm^{-3} sulfate) and listed in Table 1. The Φ of **Et-1**, **Cy-1**, and **Ph-1** is 0.055, 0.050, and 0.33 in water and 0.068, 0.052, 0.56 in DMF, respectively, similar with that of **Salen** (Φ = 0.057), **CySalen** (Φ = 0.097), and **Salphen** (Φ = 0.19) in DMF, indicating that sulfonate groups have little effect on Φ. Due to the effect of π-conjugation enhancement, the Φ of **Ph-1** and **PhMe-1** with 1,2-phenylenediamine bridges is higher than that of **Et-1** and **Cy-1**. Among all the ligands, the Φ of **PhMe-1** and **PhMe-4** is highest up to 0.56 and 0.45 in water and 0.35 and 0.60 in CH_3CN, respectively.

At room temperature, like **Salen** and **Salphen** [41], the powder of **Et-1**, **Cy-1**, and **Ph-1** emits strong blue-green, green, and yellow light with $\lambda_{em,max}$ = 494, 521, 551 nm, respectively (Table 1). Compared with in solution, both the emission and excitation spectrum of **Ph-1** in powder exhibit red shifts (Fig. S8), which is a common phenomenon for emitters in powder or solid state due to the molecular aggregation in powder or solid state.

3.4. Electronic structure calculations

To gain further insight into the nature of the excited states and to clarify the discrepancies between emission energies of the synthesized ligands, TD-DFT calculations were carried out for all the ligands with the Gaussian 03 program package (B3LYP 6-31G(d,p)) [37]. For geometry optimization, the single-crystal X-ray diffraction structures of selected ligands (phenol-imine form) are required, which were obtained or modified from published data [35,43,45–48]. The spin multiplicities of the ligands were set equal to 1. The charges of the ligands with and without sulfonate groups ($-SO_3^-$) were set equal to −2 and 0, respectively. The theoretical modeling was performed in the isolated molecule approximation ignoring the effect of the aggregation state or solvent.

The optimized structures of **Salen**, **CySalen**, **Salphen**, **Et-1**, **Cy-1**, **Ph-1**, **PhMe-1**, **PhMe-2**, **PhMe-3**, **PhMe-4**, and **CN-1** are shown in Fig. 4 and other ligands are shown in Fig. S9. In the optimized geometry of **Salphen**, the dihedral between the plane of central phenylenediamine ring and any one plane of two phenolic rings is about 28° (Fig. S5), slightly different from its single-crystal X-ray diffraction structure, in which the central phenylenediamine ring and one phenolic ring are in the same plane (Figs. S4 and S5). The optimized geometries of **Salen** and **CySalen** remain similar to their single crystal structures (Fig. S4).

Diagrams of the LUMO + 1, LUMO, HOMO, and HOMO − 1 for the ground states and the energies of frontier molecular orbitals of the selected ligands are shown in Fig. 4 and listed in Table S1, respectively, and those of other ligands are demonstrated in Fig. S9 and Table S2, respectively. For **Salen** and **CySalen** with the non-π-conjugated bridge of 1,2-ethylenediamine and 1,2-cyclohexanediamine, respectively, the HOMO and LUMO are not composed primarily of the bridges but π-functions on the two phenolic rings (Fig. 4), resulting in that **Salen** and **CySalen** have similar HOMO, LUMO levels (Table S1), UV/Vis absorption spectra, and emission spectra. On the contrary, for **Salphen** with the π-conjugated bridge of 1,2-phenylenediamine, the HOMO and LUMO are uniformly distributed in the whole molecule. The LUMO level of **Salphen** (−1.92 eV) is lower than that of **Salen** (−1.45 eV) and **CySalen** (−1.32 eV), but the HOMO level of **Salphen** (−5.67 eV) is higher than that of **Salen** (−5.95 eV) and **CySalen** (−5.86 eV). Therefore, the energy gap between HOMO and LUMO of **Salphen** (3.75 eV) is lower than that of **Salen** (4.49 eV) and **CySalen** (4.55 eV), which is in agreement with experimental data observed in UV/Vis absorption and emission spectra. The UV/Vis absorption and emission spectra of **Salphen** shows red shifts compared with those of **Salen** and **CySalen**.

The calculated LUMO + 1, LUMO, HOMO, and HOMO − 1 levels of all the selected SSLs are much higher than those of neutral **Salen**, **CySalen**, and **Salphen**. Especially, their LUMO + 1 and LUMO levels are positive, which might caused by the effect of −2 charge in the SSLs [33,49]. If the sulfonate groups were revised from $-SO_3^-$ to $-SO_3H$, the charge of the ligands would be equal to 0, which would result in no difference in the LUMO + 1, LUMO, HOMO, and HOMO − 1 spatial plots and normal levels of LUMO + 1, LUMO, HOMO, and HOMO − 1 (Fig. S10 and Table S3). The LUMO + 1 and LUMO spatial plots of **Et-1**, **Cy-1**, and **Ph-1** are similar with those of **Salen**, **CySalen**, and **Salphen**, respectively, demonstrating that the sulfonate groups in **Et-1**, **Cy-1**, and **Ph-1** have no contribution to the LUMOs. On the other hand, the sulfonate groups in **Et-1**, **Cy-1**, and **Ph-1** have obvious small contribution to the HOMO and HOMO − 1. Therefore, we tentatively assign the fluorescence transitions of **Et-1**, **Cy-1**, and **Ph-1** to $\pi \rightarrow \pi^*$(ligand) transition, mixed with n(O in sulfonate groups) → π^*(ligand) transition. However, since the contribution of sulfonate groups to the LUMO + 1, LUMO, HOMO, and HOMO − 1 is relatively small, the photophysical properties of the SSLs are similar with those of the ligands without sulfonate groups, which are consistent with the experimental data.

In order to demonstrate the effect of chemical functional groups on the frontier molecular orbitals, the frontier molecular orbital spatial plots of **Ph-1**, **PhMe-1**, **PhMe-2**, **PhMe-3**, **PhMe-4**, and **CN-1** are examined (Fig. 4). The LUMO + 1, LUMO, HOMO, and HOMO − 1 spatial plots of **Ph-1** are similar with those of **PhMe-1**, **PhMe-2**, and **PhMe-3**, revealing that methyl groups and bulky *t*-butyl groups have little contribution to the LUMO + 1, LUMO, HOMO, and HOMO − 1. However, the presence of Cl atoms in the two side phenolic rings of **PhMe-4** makes big differences in LUMO + 1, LUMO, HOMO, and HOMO − 1 spatial plots, because Cl atom is electron-rich group and donate its electron to LUMO + 1, LUMO, HOMO, and HOMO − 1. Cl atoms lead to not only the lower level of LUMO but also the lower level of HOMO, resulting in the similar energy gap with **PhMe-1** (Table S1). Therefore, based on the calculated results, **Ph-1**, **PhMe-1**, **PhMe-2**, **PhMe-3**, and **PhMe-4** should have similar emission properties, which are consistent with the experimental data. In addition, with the bridge of dicyano-1,2-ethenediamine, the HOMO (−1.034 eV) and LUMO (0.707 eV) of **CN-1** are uniformly distributed in the whole molecule with energy gap of 1.74 eV, matching well with the further red shift of

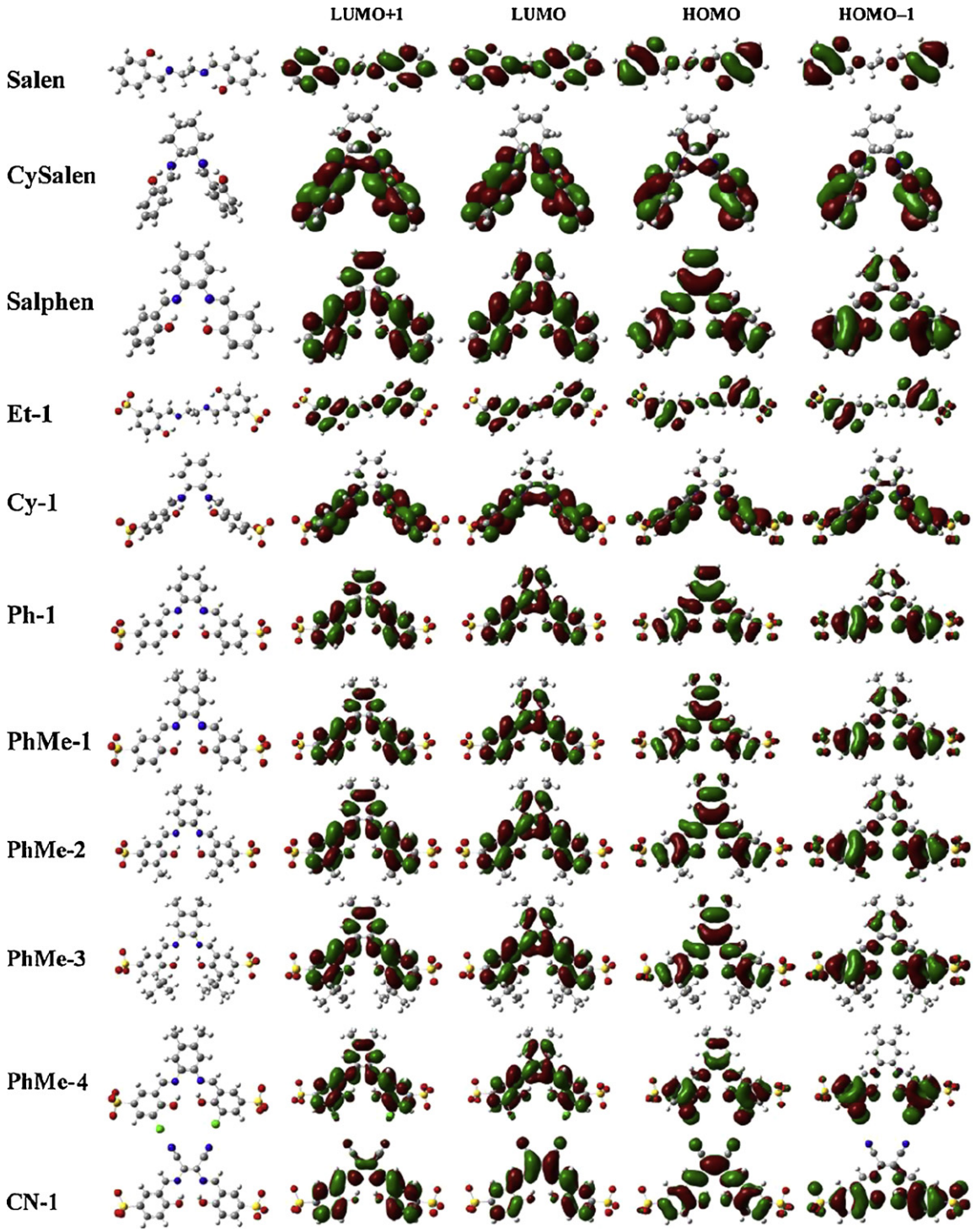

Fig. 4. Frontier molecular orbitals for the selected ligands calculated at B3LYP 6-31G(d,p) level of theory.

fluorescence ($\lambda_{em,max}$ = 563 nm in CH_3CN). The above combined results provide unequivocal confirmation not only of our structural design, but also of the photophysical nature of the tuning process.

3.5. Colorimetric analysis

The colorimetric analysis of **PhMe-4** toward various metal ions, such as Cu^{2+}, Li^{+}, K^{+}, Na^{+}, Mg^{2+}, Hg^{2+}, Fe^{3+}, Co^{2+}, Mn^{2+}, Pb^{2+}, Al^{3+}, Sr^{2+}, Ni^{2+}, Ca^{2+}, Zn^{2+}, Cr^{3+}, Ti^{3+}, Fe^{2+}, Cd^{2+}, Ce^{3+}, Ag^{+}, Bi^{3+}, and Sn^{4+} was studied. Monitored by the naked eye, the addition of 2 equiv. of the different metal ions to the colorless solution of the ligand did not show any detectable color changes. However, the drastic changes were found by UV/Vis absorption spectroscopy. For example, there is no detectable color change by the naked eye upon addition of Cu^{2+} to **PhMe-4** solution (Fig. 5), but by UV/Vis absorption spectroscopy, the absorption band at 370 nm gradually decreased following the formation of a new band centered at 350 nm upon the addition of Cu^{2+}, indicating the complexation of Cu^{2+} and **PhMe-4**.

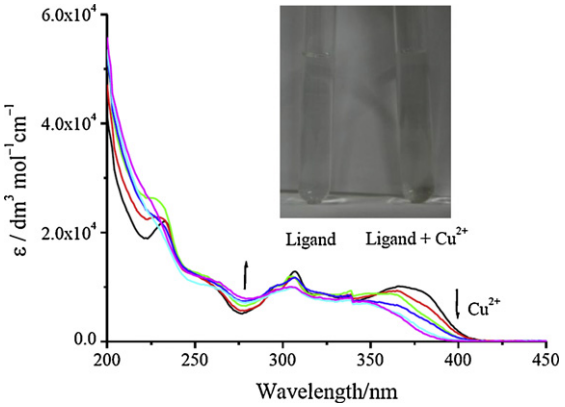

Fig. 5. Absorption spectra of **PhMe-4** (1.0×10^{-5} mol dm^{-3}) in water upon addition different equiv. of Cu^{2+} (0, 0.20, 0.60, 0.80, 1.0, 2.0). Inset photograph: **PhMe-4** in water (left) and after addition of 2.0 equiv. of Cu^{2+} (right).

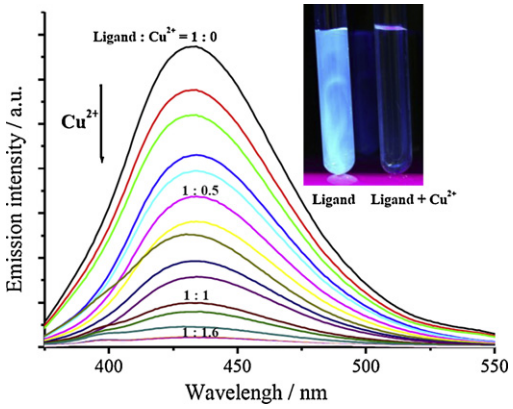

Fig. 6. Fluorescence spectra (excited at 370 nm) of **PhMe-4** (1.0×10^{-6} mol dm^{-3}) in water upon addition different equiv. of Cu^{2+} (0, 0.10, 0.20, 0.30, 0.40, 0.50, 0.60, 0.70, 0.80, 0.90, 1.0, 1.2, 1.4, 1.6, 1.8, 2.0, 2.5, 3.0, 3.5, 4.0, 5.0). Inset photograph: **PhMe-4** in water (left) and after addition of 2.0 equiv. Cu^{2+} (right) under 360 nm UV light.

3.6. *Fluorescence sensors for Cu^{2+} in water*

Considerable efforts have been made to synthesize turn-on or turn-off fluorescent probes that are selective, sensitive, and suited

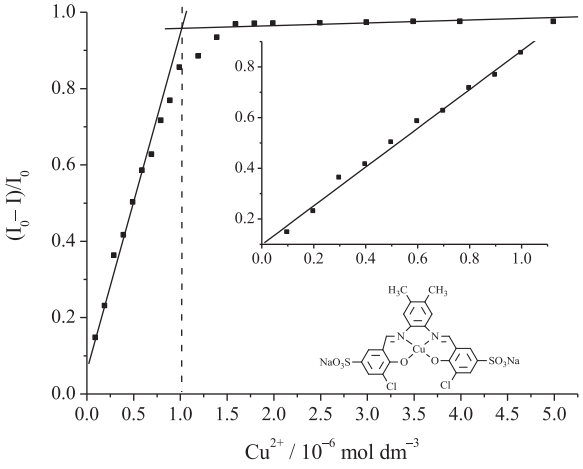

Fig. 7. Titration curve of **PhMe-4** with addition of Cu^{2+}. Inset: Job plot of **PhMe-4** with addition of Cu^{2+} and chemical structure of the **Cu(II)–PhMe-4** complex. The original concentration of **PhMe-4** was 1.0×10^{-6} mol dm^{-3} in water and the fluorescence was excited at 370 nm and measured at 435 nm.

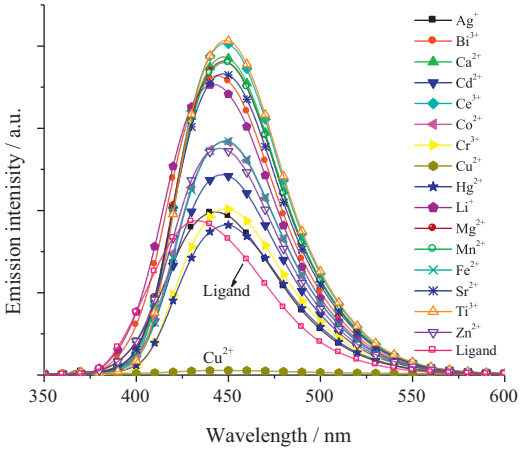

Fig. 8. Fluorescence spectra (excited at 370 nm) of **PhMe-4** (1.0×10^{-6} mol dm^{-3}) in water upon addition of 2.0 equiv. of metal ions.

to highly resolved imaging for monitoring biological processes. However, only few of them exhibit good performance in pure aqueous media, which is a very important factor for potential biological applications [50]. Moreover, some of them have shortcomings for practical applications such as cross-sensitivities toward other metal cations, low fluorescence quantum yields [51], or difficulty in tuning fluorescent wavelength. These SSLs have good stability and solubility in water with high fluorescence quantum yields and facility in tuning fluorescent wavelength, which are suitable for the application of sensing Cu^{2+} in water.

Upon addition 2 equiv. of Cu^{2+}, the fluorescence of all the SSLs was quenched (Figs. S11–23). Cu^{2+} has better quenching effect on **Ph-1**–**Ph-3** and **PhMe-1**–**PhMe-4** with 1,2-phenylenediamine bridge than **Et-1**–**Et-4**, **Cy-1**, and **Cy-2** with 1,2-ethylenediamine bridge. The fluorescence titration of **PhMe-4** with Cu^{2+} was presented in Fig. 6. The fluorescence intensity of **PhMe-4** is highly sensitive to Cu^{2+}, which will be reduced 86% and 97% upon the addition of 1 and 1.6 equiv. of Cu^{2+}, respectively. It is well known that the paramagnetic Cu^{2+} center has a pronounced quenching effect on fluorescent ligands. Copper in solution has two common oxidation states: Cu^{+} (d^{10}) and Cu^{2+} (d^{9}). Clearly, the complete filling of *d* orbitals prevents *d*–*d* metal-centered electronic transitions in Cu(I) complexes. On the contrary, such transitions are exhibited by d^9 Cu(II) complexes and lead to deactivate via ultrafast non-radiative

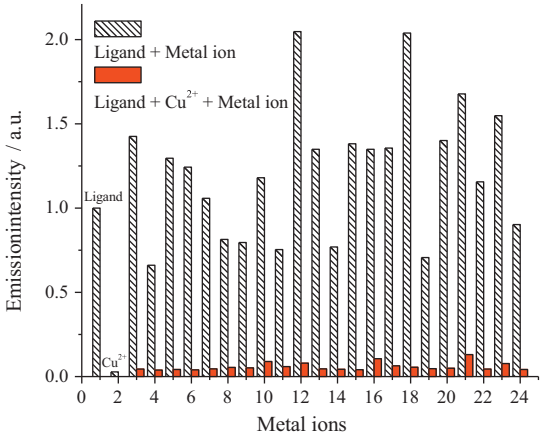

Fig. 9. Selectivity of **PhMe-4** (1.0×10^{-6} mol dm^{-3}) toward 2.0 equiv. of Cu^{2+} and other metal ions (1, ligand; 2, Cu^{2+}; 3, Li^{+}; 4, K^{+}; 5, Na^{+}; 6, Mg^{2+}; 7, Hg^{2+}; 8, Fe^{3+}; 9, Co^{2+}; 10, Mn^{2+}; 11, Pb^{2+}; 12, Al^{3+}; 13, Sr^{2+}; 14, Ni^{2+}; 15, Ca^{2+}; 16, Zn^{2+}; 17, Cr^{3+}; 18, Ti^{3+}; 19, Fe^{2+}; 20, Cd^{2+}; 21, Ce^{3+}; 22, Ag^{+}; 23, Bi^{3+}; 24, Sn^{4+}). In these experiments, the fluorescence was excited at 370 nm and measured at 435 nm.

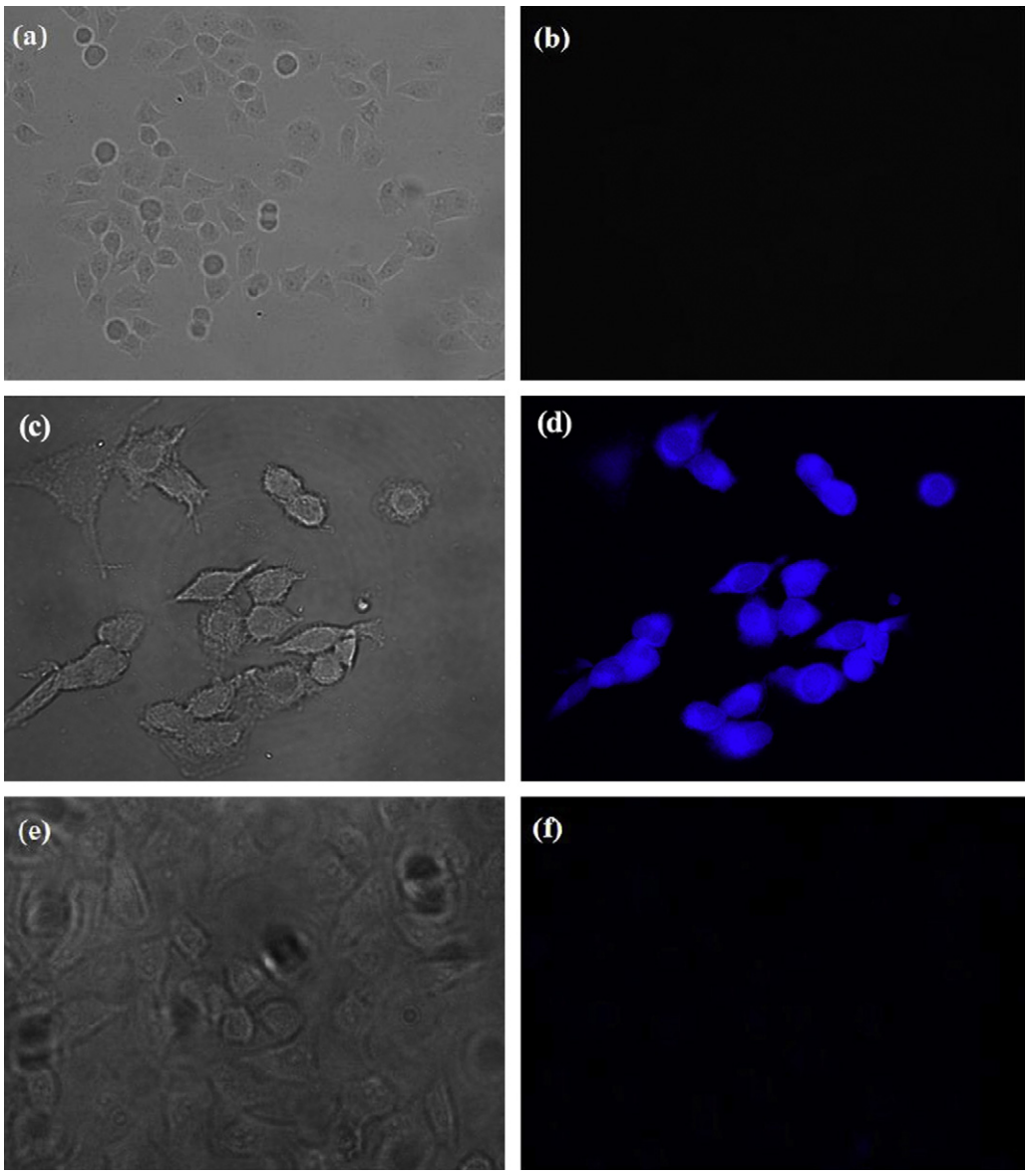

Fig. 10. Brightfield (a) (400×) and fluorescence images (b) of A549 cells in PBS; brightfield (c) and fluorescence images (d) of cells + **PhMe-4** in PBS; brightfield (e) and fluorescence images (f) of cells + **PhMe-4** + Cu^{2+} in PBS.

processes, resulting in that the most luminescent Cu complexes are not Cu(II) complexes but Cu(I) complexes [52].

The fluorescence intensity of **PhMe-4** exhibits gradual reduction upon the addition of 0–1 equiv. of Cu^{2+} and saturation upon the addition of 1.6–5.0 equiv. of Cu^{2+} (Fig. 7), revealing that the stoichiometry of complex formed between the ligand and Cu^{2+} ions is 1:1, which is consistent with the former reported result [20,24,30,31]. The association constant (K_a) of the resulting complex was found to be 1.61×10^6 dm^3 mol^{-1}, which was evaluated by fitting the fluorescence intensity–metal ion molar ratio data to a 1:1 model using a nonlinear least-squares curve-fitting program. As shown in the inset photograph of Fig. 8, a good linearity (correlation coefficient $R^2 = 0.996$, $n = 10$) of the fluorescence intensity as the function of the concentration of Cu^{2+} between 0 and 1.0×10^{-6} mol dm^{-3} is established. The detection limit, based on the definition by IUPAC ($C_{DL} = 3$ Sb/m) [53], was found to be 8.4 nmol dm^{-3} (0.54 ppb) from 10 blank solutions. To the best of our knowledge, this value is one of the most sensitive fluorescence sensors for Cu^{2+} in aqueous media and much lower than the national primary drinking water regulation for copper (1.3 ppm) set by U.S. EPA [54], indicating that **PhMe-4** is suitable to be highly sensitive Cu^{2+} chemosensor in water.

The selectivity behavior is obviously one of the most important characteristics of a chemosensor, that is, the relative sensor response for the primary ion over other ions present in solution. In order to evaluate the selectivity of **PhMe-4**, other 22 different kinds of metal ions (Li^+, K^+, Na^+, Mg^{2+}, Hg^{2+}, Fe^{3+}, Co^{2+}, Mn^{2+}, Pb^{2+}, Al^{3+}, Sr^{2+}, Ni^{2+}, Ca^{2+}, Zn^{2+}, Cr^{3+}, Ti^{3+}, Fe^{2+}, Cd^{2+}, Ce^{3+}, Ag^+, Bi^{3+}, and Sn^{4+}) which probably interfere with the detection of Cu^{2+} were performed under the similar conditions: the concentrations of **PhMe-4** were all kept at 1.0×10^{-6} mol dm^{-3} and 2 equiv. of metal ions were added. As depicted in Figs. 8 and 9, Cu^{2+} gave almost 100% quench of the fluorescence intensity at 435 nm, the other metal ions showed slight fluorescence quenching or enhancement. In addition, competition experiments were also performed in the presence of **PhMe-4** and 2 equiv. of Cu^{2+} mixed with 2 equiv. of the other metal ions (Fig. 9) to explore practical applicability of **PhMe-4** as a Cu^{2+}-selective fluorescence chemosensor. The fluorescence intensity of solutions containing both Cu^{2+} and the other metal ions shows no obvious variation compared with those containing only

Cu^{2+}. The combined results reveal that **PhMe-4** can detect Cu^{2+} with minimum interference from other metal ions and is a good Cu^{2+} sensor.

3.7. Living cell imaging

Fluorescence sensors that can selectively monitor specific metal ions in living cells have been indispensable tools for understanding of biological phenomena. In order to evaluate the possibility of **PhMe-4** as a fluorescence probe to image Cu^{2+} in living cells, **PhMe-4** was firstly used to culture A549 cells in phosphate buffered saline (PBS) for 20 min. Through fluorescence microscope, the untreated A549 cells showed no fluorescence, as shown in Fig. 10b. After sole incubation of A549 cells with **PhMe-4**, strong blue intracellular fluorescence (Fig. 10d, excited at 370 nm) was observed, indicating that **PhMe-4** could be used as fluorescence probe for imaging living cell. Upon further addition of Cu^{2+}, the blue fluorescence was nearly 90 percent quenched (Fig. 10f). The combined results reveal that **PhMe-4** is suitable for fluorescence probe to image Cu^{2+} in living cells.

4. Conclusion

We have synthesized and studied the photophysical properties of a series of water-soluble sulfonato-Salen-type ligands. The presence of sulfonate groups in the SSLs ensures not only good stability but also solubility in water without affecting the excited state properties. The photophysical properties of the ligands with sulfonate groups are similar with those of the ligands without sulfonate groups. The further TD-DFT calculations demonstrate that the contribution of sulfonate groups to the HOMOs and LUMOs is relatively small. The SSLs exhibit strong blue, green, or orange fluorescence in water, which can be selectively quenched by Cu^{2+}. Therefore, these water-soluble SSLs represent good candidates for development toward highly selective and sensitive fluorescence sensor for the detection of Cu^{2+} in water and living cells. The main focus of this work is not only on achieving an excellent Cu^{2+} probe but also on studying photophysical properties of these ligands. Although there have been a lot of published papers that described Cu^{2+} sensing in water, we have demonstrated an alternative way by introducing sulfonate groups to the ligand to achieve water-soluble fluorescence sensors.

Acknowledgements

This work was supported by the National Natural Science Foundation of China (nos.: 21172160, 20901052, 30971070, and NCET-10-0581) and Ministry of Education of China (no. 20100181120039). We thank the Analytical & Testing Centre of Sichuan University for NMR analysis and Prof. X.Q. Yu, College of Chemistry, Sichuan University, for fluorescence measurement.

Appendix A. Supplementary data

Supplementary data associated with this article can be found, in the online version, at http://dx.doi.org/10.1016/j.aca.2012.05.022.

References

[1] P.G. Lacroix, Eur. J. Inorg. Chem. (2001) 339–348.
[2] M.J. O'Donnell, Acc. Chem. Res. 37 (2004) 506–517.
[3] E. Hadjoudis, I.M. Mavridis, Chem. Soc. Rev. 33 (2004) 579–588.
[4] K.C. Gupta, A.K. Sutar, Coord. Chem. Rev. 252 (2008) 1420–1450.
[5] F. Faridbod, M.R. Ganjali, R. Dinarvand, P. Norouzi, S. Riahi, Sensors 8 (2008) 1645–1703.
[6] M. Andruh, Chem. Commun. 47 (2011) 3025–3042.
[7] L. Canali, D.C. Sherrington, Chem. Soc. Rev. 28 (1999) 85–93.
[8] P.G. Cozzi, Chem. Soc. Rev. 33 (2004) 410–421.
[9] H. Miyasaka, A. Saitoh, S. Abe, Coord. Chem. Rev. 251 (2007) 2622–2664.
[10] A.W. Kleij, Eur. J. Inorg. Chem. (2009) 193–205.
[11] E. Lamour, S. Routier, J.L. Bernier, J.P. Catteau, C. Bailly, H. Vezin, J. Am. Chem. Soc. 121 (1999) 1862–1869.
[12] P. Wu, D.L. Ma, C.H. Leung, S.C. Yan, N.Y. Zhu, R. Abagyan, C.M. Che, Chem. Eur. J. 15 (2009) 13008–13021.
[13] P.F. Wang, Z.R. Hong, Z.Y. Xie, S.W. Tong, O.Y. Wong, C.S. Lee, N.B. Wong, L.S. Hung, S.T. Lee, Chem. Commun. (2003) 1664–1665.
[14] Y. Zhou, J.W. Kim, M.J. Kim, W.J. Son, S.J. Han, H.N. Kim, S. Han, Y. Kim, C. Lee, S. Kim, D.H. Kim, J.J. Kim, J. Yoon, Org. Lett. 12 (2010) 1272–1275.
[15] K.Y. Hwang, M.H. Lee, H. Jang, Y. Sung, J.S. Lee, S.H. Kim, Y. Do, Dalton Trans. (2008) 1818–1820.
[16] C.M. Che, S.C. Chan, H.F. Xiang, M.C.W. Chan, Y. Liu, Y. Wang, Chem. Commun. (2004) 1484–1485.
[17] H.F. Xiang, C.N. Li, S.C. Yu, C.M. Che, P.T. Lai, P.C. Chui, Proc. SPIE 5519 (2004) 218–225.
[18] H.F. Xiang, S.C. Chan, K.K.Y. Wu, C.M. Che, P.T. Lai, Chem. Commun. (2005) 1408–1410.
[19] C.M. Che, C.C. Kwok, S.W. Lai, A.F. Rausch, W.J. Finkenzeller, N.Y. Zhu, H. Yersin, Chem. Eur. J. 16 (2010) 233–247.
[20] S.C. Wang, G.W. Men, L.Y. Zhao, Q.F. Hou, S.M. Jiang, Sens. Actuators B: Chem. 145 (2010) 826–831.
[21] D. Udhayakumari, S. Saravanamoorthy, M. Ashok, S. Velmathi, Tetrahedron Lett. 52 (2011) 4631–4635.
[22] Y. Zhou, H.N. Kim, J. Yoon, Bioorg. Med. Chem. Lett. 20 (2010) 125–128.
[23] Y. Dong, J.F. Li, X.X. Jiang, F.Y. Song, Y.X. Cheng, C.J. Zhu, Org. Lett. 13 (2011) 2252–2255.
[24] C. Gou, S.H. Qin, H.Q. Wu, Y. Wang, J. Luo, X.Y. Liu, Inorg. Chem. Commun. 14 (2011) 1622–1625.
[25] X. Chen, M.J. Jou, H. Lee, S. Kou, J. Lim, S.W. Nam, S. Park, K.M. Kim, J. Yoon, Sens. Actuators B: Chem. 137 (2009) 597–602.
[26] A.K. Mahapatra, G. Hazra, N.K. Das, S. Goswami, Sens. Actuators B: Chem. 156 (2011) 456–462.
[27] M. Hosseini, M.R. Ganjali, B. Veismohammadi, S. Riahi, P. Norouzi, M. Salavati-Niasari, S.D. Abkenar, Anal. Lett. 42 (2009) 1029–1040.
[28] Y. Zhou, J.Y. Jung, H.R. Jeon, Y. Kim, S.J. Kim, J. Yoon, Org. Lett. 13 (2011) 2742–2745.
[29] A.K. Mahapatra, J. Roy, P. Sahoo, S.K. Mukhopadhyay, A. Chattopadhyay, Org. Biomol. Chem. 10 (2012) 2231–2236.
[30] Z.Q. Wu, Z.Q. Jiang, D. Wu, H.F. Xiang, X.G. Zhou, Eur. J. Org. Chem. (2010) 1854–1857.
[31] Y.Y. Qu, F. Ke, L. Zhou, Z.K. Li, H.F. Xiang, D. Wu, X.G. Zhou, Chem. Commun. 47 (2011) 3912–3914.
[32] N.C. Maiti, S. Mazumdar, N. Periasamy, J. Phys. Chem. B 102 (1998) 1528–1538.
[33] S.Y. Ma, Chem. Phys. Lett. 332 (2000) 603–610.
[34] K.J. Berry, F. Moya, K.S. Murray, A.B. van der Bergen, B.O. West, J. Chem. Soc., Dalton Trans. (1982) 109–116.
[35] É. Delahaye, M. Diop, R. Welter, M. Boero, C. Massobrio, P. Rabu, G. Rogez, Eur. J. Inorg. Chem. (2010) 4450–4461.
[36] J.N. Demas, G.A. Crosby, J. Phys. Chem. 75 (1971) 991–1024.
[37] M.J. Frisch, G.W. Trucks, H.B. Schlegel, G.E. Scuseria, M.A. Robb, J.R. Cheeseman, J.A. Montgomery Jr., T. Vreven, K.N. Kudin, J.C. Burant, J.M. Millam, S.S. Iyengar, J. Tomasi, V. Barone, B. Mennucci, M. Cossi, G. Scalmani, N. Rega, G.A. Petersson, H. Nakatsuji, M. Hada, M. Ehara, K. Toyota, R. Fukuda, J. Hasegawa, M. Ishida, T. Nakajima, Y. Honda, O. Kitao, H. Nakai, M. Klene, X. Li, J.E. Knox, H.P. Hratchian, J.B. Cross, V. Bakken, C. Adamo, J. Jaramillo, R. Gomperts, R.E. Stratmann, O. Yazyev, A.J. Austin, R. Cammi, C. Pomelli, J.W. Ochterski, P.Y. Ayala, K. Morokuma, G.A. Voth, P. Salvador, J.J. Dannenberg, V.G. Zakrzewski, S. Dapprich, A.D. Daniels, M.C. Strain, O. Farkas, D.K. Malick, A.D. Rabuck, K. Raghavachari, J.B. Foresman, J.V. Ortiz, Q. Cui, A.G. Baboul, S. Clifford, J. Cioslowski, B.B. Stefanov, G. Liu, A. Liashenko, P. Piskorz, I. Komaromi, R.L. Martin, D.J. Fox, T. Keith, M.A. Al-Laham, C.Y. Peng, A. Nanayakkara, M. Challacombe, P.M.W. Gill, B. Johnson, W. Chen, M.W. Wong, C. Gonzalez, J.A. Pople, Gaussian 03, Revision E.01, Gaussian, Inc., Wallingford, CT, 2004.
[38] H.J. Wories, J.H. Koek, G. Lodder, J. Lugtenburg, Recl. Trav. Chim. Pays-Bas 104 (1985) 288–291.
[39] S. Di Bella, I. Fragala, I. Ledoux, M.A. Diaz-Garcia, T.J. Marks, J. Am. Chem. Soc. 119 (1997) 9550–9557.
[40] R.C. Felicio, E.T.G. Cavalheiro, E.R. Dockal, Polyhedron 20 (2001) 261–268.
[41] O.V. Kotova, S.V. Eliseeva, A.S. Averjushkin, L.S. Lepnev, A.A. Vaschenko, A.Y. Rogachev, A.G. Vitukhnovskii, N.P. Kuzmina, Russ. Chem. Bul. Int. Ed. 57 (2008) 1880–1889.
[42] O.K. Abou-Zied, Chem. Phys. 337 (2007) 1–10.
[43] E. Tozzo, S. Romera, M.P.D. Santos, M. Muraro, R.H.D.A. Santos, L.M. Liao, L. Vizotto, E.R. Dockal, J. Mol. Struct. 876 (2008) 110–120.
[44] S.A. Beyramabadi, A. Morsali, Int. J. Phys. Sci. 6 (2011) 1780–1788.
[45] N.B. Pahor, M. Calligaris, G. Nardin, L. Randaccio, Acta Cryst. B34 (1978) 1360–1363.
[46] S.S. Sun, C.L. Stern, S.T. Nguyen, J.T. Hupp, J. Am. Chem. Soc. 126 (2004) 6314–6326.
[47] X.P. Yang, R.A. Jones, Q.Y. Wu, M.M. Oye, W.K. Lo, W.K. Wong, A.L. Holmes, Polyhedron 25 (2006) 271–278.
[48] T.Z. Yu, K. Zhang, Y.L. Zhao, C.H. Yang, H. Zhang, L. Qian, D.W. Fan, W.K. Dong, L.L. Chen, Y.Q. Qiu, Inorg. Chim. Acta 361 (2008) 233–240.

[49] M. Sugimoto, M. Anzai, K. Sakanoue, S. Sakaki, Appl. Phys. Lett. 79 (2001) 2348–2350.
[50] H.H. Wang, L. Xue, Z.J. Fang, G.P. Li, H. Jiang, New J. Chem. 34 (2010) 1239–1242.
[51] S. Yin, V. Leen, S.V. Snick, N. Boens, W. Dehaen, Chem. Commun. 46 (2010) 6329–6331.
[52] N. Armaroli, G. Accorsi, F. Cardinali, A. Listorti, Top. Curr. Chem. 280 (2007) 69–115.
[53] L.A. Currie, Anal. Chim. Acta 391 (1999) 105–126.
[54] U.S. EPA. EPA 816-F-09-0004, May 2009.